第 38 卷第 1 期
2019 年 2 月

红 外 与 毫 米 波 学 报
J. Infrared Millim. Waves

Vol. 38, No. 1
February, 2019

文章编号: 1001 - 9014(2019)01 - 0021 - 06

DOI: 10.11972/j.issn.1001 - 9014.2019.01.004

Theoretical study on the far-infrared perfect absorbers with SU8 based multilayered metamaterial structure

HU Zhi-Ting[1,2], CHEN Ji-Wei[2,3], DU Lei[2], ZHU Yu-Fang[3],
ZHANG Jia-Zhen[2], XU Huang[2], LIU Feng[1], CHEN Gang[2*]

(1. Shanghai Normal University, Shanghai 200234, China;
2. State Key Laboratory of Infrared Physics, Shanghai Institute of Technical Physics, Chinese Academy of Sciences, Shanghai 200083, China;
3. School of Materials Science and Engineering, University of Shanghai for Science and Technology, Shanghai 200093, China)

Abstract: A theoretical study on the perfect absorbers working in the far-infrared region with SU8 based multiple-layer metamaterials has been demonstrated. The perfect absorbers consist of periodic array of metal particles, SU8 dielectric spacing layer and a thicker metallic bottom layer. Through the LC model and the finite element numerical simulation methods, we studied the performance of the absorber. With finely tuned parameters, such like the thickness of the SU8 dielectric layers, the periodicity of the metal particles array, and the length of the metal particles, the near perfect absorption up to ~100% at the wavelength range between 20 μm to 30 μm for far infrared can be achieved. Based on these results, further design for the double-resonator absorber has been provided. Dual band perfect absorption can be accurately and independently obtained by adjusting the particle size of the upper and the lower metal layers. Moreover, the wavelength of the perfect absorption is also almost independent of the incident angle. These phenomena can be attributed to the multiple reflections between the thick metallic bottom layer and metal particle layers separated by SU8 dielectric layer, which can also be explained using a LC model as the resonant absorption in the metal-dielectric-metal cavities.

Key words: metamaterial, perfect absorber, far-IR, SU8
PACS: 41.20.Jb, 78.20.Ci

基于 SU8 的远红外超材料完美吸收器理论研究

胡之厅[1,2], 程纪伟[2,3], 杜 磊[2], 朱钰方[3], 张家振[2], 徐 煌[2], 刘 锋[1], 陈 刚[2*]

(1. 上海师范大学, 上海 200234;
2. 中国科学院上海技术物理研究所 红外物理国家重点实验室, 上海 200083;
3. 上海理工大学 材料科学与工程学院, 上海 200093)

摘要: 设计了一种基于 SU8 介质材料的工作波段为 20-30 微米范围内的的多层超材料吸收器. 该吸收器由金属颗粒周期阵列、介质间隔层和金属底层组成. 利用 LC 模型和 FDTD 数值模拟方法, 通过对 SU8 介质层厚度、金属颗粒阵列周期、金属颗粒尺寸等参数的优化, 实现了对 20-30 微米波段范围内入射波的接近 100% 的完美吸收. 并在上述研究基础上进一步设计了具有双层谐振腔的双模完美吸收器. 通过数值模拟发现, 由于 SU8 介质间隔层厚度的增加, 上下两个谐振吸收器可以分别独立实现对特定波长的完美吸收. 相应的特征共振吸收波长符合 LC 模型的预测. 同时, 数值模拟结果进一步证实了共振吸收频率与入射角度无关. 该完美吸收机制可以归因于入射光在金属底层-SU8 介质层-金属颗粒层所组成的谐振腔内多次反射吸收.

关 键 词: 超材料; 完美吸收器; 远红外; *SU8*

中图分类号: O469 **文献标识码:** *A*

Received date: 2018-06-10, **revised date:** 2018-12-26 **收稿日期:** 2018-06-10, **修回日期:** 2018-12-26

Foundation items: Supported by the National Natural Science Foundation of China (No. 61474130 and No. 51572172), the Scientific Development Project of University of Shanghai for Science and Technology (16KJFZ011), and Chinese Academy of Sciences via Hundred Talents Program

Biography: HU Zhi-Ting (1992-), male, Shangrao, Chian. master. Research area involves Semiconductor materials and photodetectors. E-mail: huzhiting1227@sina.com

* **Corresponding author:** E-mail: gchen@mail.sitp.ac.cn

Introduction

Far-infrared photodetecting and imaging have attracted great attention due to the broad applications in biomedicine [1], environmental remote sensing [2], explosives detection [3], materials characterization [4,5], and astronomy [6]. To improve the signal-to-noise ratio of the current far-infrared photodetectors, especially the bolometers, significant enhancement of the photo absorption at far infrared wavelength is required. Recently, metamaterial absorbers have been extensively studied as the potential absorptive coatings for the photodetectors and bolometers, owing to their excellent performance at far-infrared band [7-17]. It has been demonstrated that polarization independent and omnidirectional absorption can be achieved for thin MAs [7-24]. A traditional MAs is made of a periodically patterned metallic layer, a dielectric spacing layer and a thick metal layer, where can generate resonances for achieving frequency-selective light absorption. The metallic pattern includes split ring resonators (SRR) [7-16], crosses [18], particles and rectangles [19-21]. The absorption band width, polarization dependence, and spectral line shape can be varied by adjusting the structure of absorber. Meanwhile traditional dielectric spacing layers are usually thin films prepared with both PECVD deposition and plasma etching procedures. In this work, we used the epoxy-based negative photoresist SU8 as a structural material, offer possibilities for quick, stable, simple microfabrication of far infrared and THz imaging detectors. SU-8 is a low-cost material that can quickly be spun onto a substrate at a wide range of thicknesses and photolithographically patterned into a variety of structures, which dramatically increasing the speed and lowering the cost of production for opto-electronic devices. Moreover it can also provide a self-leveling capability, which is required by the MA fabrications. Based on this structure, we have studied the dependence of the MA maximum and the wavelength at far-infrared region on the SU8 spacer layer thickness, with both the numerical simulation and the LC circuit modeling based on interference theory.

1 Methods and modeling

A variety of mechanisms for the resonant absorption have been proposed. In the metamaterials approach, the permitivity and permeability are used to describe the macroscopic electrodynamics. In this case, electromagnetic resonances can generate a surface impedance to match free space, a spatially averaged surface, which is over the sub-wavelength structures, have strong dispersion [7-16]. On the other hand, interference approach that assumes two kinds of metallic layers are linked to multiple reflections and superposition, similar to the case of Fabry-Perot resonances [23].

In this work, we first adopted the LC equivalent circuit method [24] which is a unifying approach to obtain the desired parameters for the MAs working on the far-infrared range with the wavelength at about 20 ~ 30 μm. In this case, when light illuminate on the MA, a pair of anti-parallel current will generate in the periodic array of metallic particles and metal bottom layer [25]. Therefore, it emerges an electric current loop. In other words, one unit cell of metamaterial corresponds to a "closed wire loop". Because the magnetic moment induced by the current loop can strongly interact with the magnetic field of incident light, it is often called a magnetic resonance. Furthermore, the electric current loop can be described by a LC equivalent circuit model [26]. The resonant absorption will be achieved, if the frequency of the external light can match with the intrinsic frequency of resonators. On the other hand, the intrinsic frequency of resonator can be quantitatively described by circuit elements of the LC equivalent circuit model.

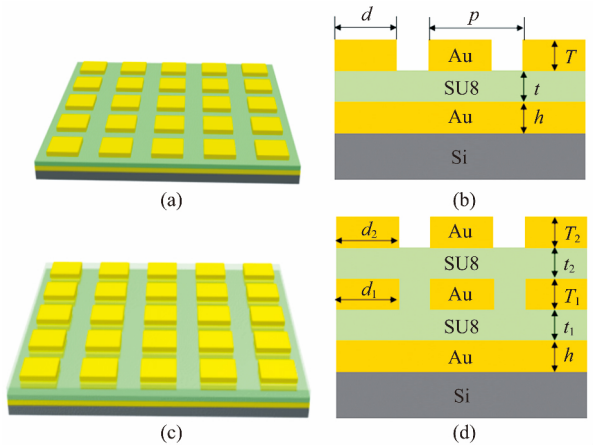

Fig. 1 (a) and (c) are the schematic structure for the metamaterial perfect absorbers with single-resonant cavity and double-resonant cavities respectively, (b) and (d) are the respective cross-sectional profiles for structure (a) and (c)

图1 (a)和(c)分别是单谐振腔和双谐振腔超材料吸收器的结构,(b)和(d)分别是(a)和(c)的截面轮廓

The MA structure discussed in the LC equivalent circuit model, with single bandwidth, is composed of particle resonators as shown in Fig. 1(a) and 1(b). The effect of interaction between the periodic array of metal particles and thicker metallic bottom layer can be expressed by a parallel plate capacitor of $C_m = \varepsilon_0 \varepsilon_d \sigma_{eff} / t$, and a parallel plate inductance of $L_m = \mu_0 d_{eff} t / (2d)$. Here ε_0 and ε_d is the permitivity for vacuum and the dielectric medium respectively. And μ_0 is the permeability of vacuum, σ_{eff} is the effective area for the resonator, t is the thickness of dielectric layer, and $d_{eff} = d$ is the effective length of the resonator. The interaction of the neighboring resonators can be modeled as a gap capacitor with, $C_g = \pi \varepsilon_0 d / In(g/t)$, where g is the interval distance of resonators. Therefore, the intrinsic frequency ω_r can be simplified as $\omega_r = 1/(L_m C_m)^{1/2}$ for $C_g \approx 0.1 C_m$, considering the geometry and material parameters used here. Thus the relational expression between the wavelength of resonant peak and the dielectric constant of dielectric layer can be given by $\lambda = 2\pi d (\alpha \varepsilon_d / 2)^{1/2}$, here α is the effective area ratio for the resonator.

With this expression, we determined the basic structures and the parameters for the far-infrared perfect absorbers. The SU8/Au multi-layer structure were adopt-

ed which is different from the traditional triple-layer MAs. Two types of configurations were proposed here. One is a three-layer structure, with a thicker metallic layer, a dielectric layer and a layer of periodic array of metallic particles, as shown in Figure 1(a) and 1(b). In this structure, the thicker metallic bottom layer is used as a reflective layer. The metallic particles are periodically patterned on the top of a dielectric layer, which can form a resonant cavity with the metallic bottom layer. Another one is five-layer structure, as shown in Figure 1(c) and 1(d). There are two resonant cavities in this configuration formed by two layers of periodic array of metal particles separated by dielectric layers, respectively. In these models, h, t, T are the thickness of Au back layer, dielectric SU8 layer, and Au particle particle layers, respectively. p is the periodicity of the Au particle. And d is the edge length of the Au particle. In this work, the h is fixed at 150 nm.

Based on these models,, numerical simulations with FDTD solution were then used to perform the further study on the behavior of the MAs. In the simulations, the complex permitivity of Au is described by the Drude model, with the plasma frequency $\omega_p = 2\pi \times 2\,895$ THz and the collision frequency $\omega_r = 2\pi \times 15.5$ THz [27]. Periodic boundary conditions were employed for the X-Y plane, and a plane wave of TM polarization (with magnetic field H perpendicular to the X-Z plane) was normally illuminated upon the structure as the excitation source. The frequency-dependent absorption was obtained from the S-parameters by $A(\omega) = 1 - T(\omega) - R(\omega) = 1 - S_{21}^2 - S_{11}^2$, where S_{21} and S_{11} are the frequency-dependent transmission and reflection coefficients, respectively. Since the thickness of Au back plane is fixed as 150 nm which is enough to limit all of the transmission light $T(\omega) = 0$, the absorption coefficient can be simplified as $A(\omega) = 1 - R(\omega)$.

2 Results and discussions

In Fig. 2(a), the absorption spectra of the MA with single-resonant cavity are attained by varying the thickness of SU8 dielectric layer, while the metal particle periodicity p, the metal length d, and the top metal thickness T are fixed at 10 μm, 5 μm, and 60 nm respectively. It is obviously observed that the thickness of dielectric layer has significant influence on the absorption rate of MA. When t is 300 nm, the absorption reaches the maximum. On the other hand, when the thickness of dielectric layer is far away the optimum value, the absorptance decreases sharply. For example, when the thickness of metamaterial is 300 nm, it could achieve an absorption rate near 100%, but only 53% for 100 nm, and about 33% for 800 nm. This is due to the fact that with the dielectric layer thickness increasing, the equivalent capacitance has changed, and mismatch with the impedance at free space. It leads an imperfect absorption, and the same as thickness decreasing. In Fig. 2(b) we found that the thickness of the top metal particle has almost no significant influence on the absorptance when it varies from 40 to 100 nm. Furthermore, we investigate the effect of the particle length d, s on the absorptance of the MA with the periodicity p being fixed at 10 μm, and the dielectric thickness being fixed at the optimized value of 300 nm, as shown in Fig. 2(c). It can be seen that with the increase of the length of metal particles from 4 to 8 μm, a red shift of the maximal absorptance from 16 to 34 μm occurs, while the absorption rate is almost unchanged. Meanwhile at the short wavelength end, there is a significant peak existing for every main absorptance peak, which is attributed to the diffraction peak owing to their similar position as the periodicity of the gold particle. In Fig. 2(d), we fixed the gold particle length as 6 μm, and varied the periodicity of the gold particles. In this case, we found the maximal wavelength of the main absorptance peak almost fixed at about 23 μm. Meanwhile, the diffraction peaks show a significant dispersion with the varying of the periodicity, which is due to the fact that diffraction peak position is exactly determined by the periodicity of the patterning, which thus is masked with gray bar in Figure 2 and Figure 4. Therefore it can be concluded that the thickness and the periodicity of the metal particles have rather little influence on the position of the maximal absorptance.

In Figure 3, we further show the influence of incident angle of the electromagnetic wave on the absorptance with the parameters of the MA: t is fixed at $t = 300$ nm, $p = 10$ μm, and $d = 6$ μm. From the simulation result, when the incident angle is smaller than 40°, there is rather little influence on the absorptance. Only when the incident angel exceeds 50°, a prominent broadening of the absorption peak, as well as the gradual deterioration of the absorptance can be observed. Even though the absorptance of >85% can still be achieved as the incident angle is about 60°.

From the results simulated above, the absorption spectrum of single-resonant layer is relatively narrow, and it is hard to achieve a broadband or multi-band absorption by changing geometric parameter. Therefore, in order to obtain a structure of MA which can behave as a broadband or multi-band absorption in far infrared wavelength, we proposed the MA structures with double resonant layers. The schematic and the profile of the double-resonant layers absorber is shown in Fig. 1(c) and (d). Based on this design, the effects of different geometric parameters on absorptance have also been investigated via the numerical simulations.

Figure 4(a) shows the simulated absorption spectra with the varying thickness $t_1 = t_2$, for the double resonant MA with the parameters $p = 10$ μm, and $d = 6$ μm. For the given parameters, the maximum of the absorptance occurs at about 22 μm with the optimized dielectric thickness $t_1 = t_2 = 1\,000$ μm as drown in blue. Obviously for the double resonator absorber the varying of the dielectric thickness can also make a great difference in absorptance as predicted by the LC model. There is a significant difference is that, for the double-resonator absorber, the optimized dielectric layer is much thicker than that of the single resonator absorber. The magnetic field distribution in Fig. 5(a) shows both resonators contribute to the absorption. Besides the main peak, there is another peak appears at about 30.5 μm, which is attributed to the double resonant layers as shown in Fig. 5(b). For all other value of t, there are the 2nd peaks existing at the longer wavelength side. On the other hand,

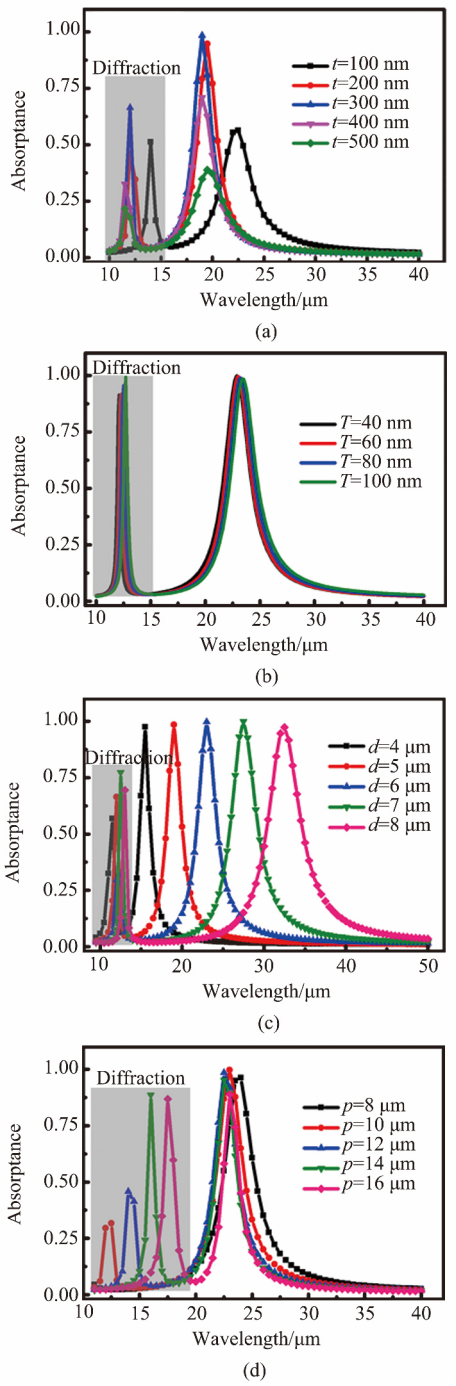

Fig. 2 The simulated absorption spectrum of single-resontant layer metamaterial for varying the thickness of dielectric layer (a) (d = 5 μm, p = 10 μm, T = 60 nm) and gold layer (b) (d = 6 μm, p = 10 μm, t = 300 nm), the side lengths of gold particle (c) (T = 60 nm, p = 10 μm, t = 300 nm), the periods of gold particle (d) (d = 6 μm, h = 150 nm, t = 300 nm, T = 60 nm)

图2 计算得到的单谐振腔超材料吸收器的吸收光谱,对应于不同的介质层厚度(a)(d = 5 μm, h = 150 nm, T = 60 nm),金属厚度(b)(d = 6 μm, p = 10 μm, h = 150 nm, t = 300 nm),金属块边长(c)(T = 60 nm, p = 10 μm, h = 150 nm, t = 300 nm)和金属块的周期(d)(d = 6 μm, h = 150 nm, t = 300 nm, T = 60 nm)

with the p is fixed at p = 10 μm, and $t_1 = t_2$ = 1 000 μm,

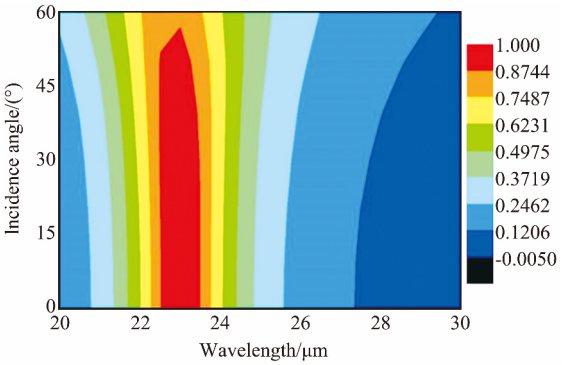

Fig. 3 Aborptance as a function of wavelength and the incident angle of light for single-resonant layer absorber

图3 单谐振腔吸收器中吸收率与入射光波长和角度的关系

the red shift of both the main peak and the second peak of the absorptance maximum can also be observed as shown in Fig. 4(b). As periods of metal particles increase from 8 μm to 12 μm, while the width keeps 6 μm constantly, the absorption rate and absorption peak has almost unchanged as shown in Fig. 4(c). This is well consistent with the results of theoretical derivation.

Obviously, to achieve higher absorptance for the second absorption maximal peak, the length of the metal particles has to be further optimized to achieve a dual-band absorption at far infrared wavelength. The results have been shown in Fig. 4(d), the occurrence of near 100% dual-band absorption can be ascribed to the optimization of the particle length d_1 for the bottom particle and d_2 for the top particle. All the other parameters are fixed as $t_1 = t_2$ = 1 000 nm, and p = 10 μm. As the length of the metal particles at the bottom and top layers are 5 μm and 7 μm, ie., d_1 = 7 μm and d_2 = 5 μm, respectively. It can generate a dual-band absorption, absorptance close to 100% at 18 μm and 26 μm, as indicated by the black lines in Fig. 4(d). Nevertheless, if the d_1 is set to be 8 μm, the second maximal peak is shifted to 30.5 μm as indicated by the red line in Fig. 4(d). We also investigated the other two cases, ie. d_1 = 7 μm, d_2 = 6 μm, and d_1 = 8 μm, d_2 = 6 μm, respectively, as indicated with green and blue lines in Fig. 4(d). Again for the case of d_1 = 7 μm, d_2 = 6 μm, we achieve the dual maximum at 22 and 26 μm. And for the case of d_1 = 8 μm, d_2 = 6 μm, the dual maxima at 22 and 30.5 μm are obtained. Further study on the magnetic field distribution profile as shown in Fig. 5(c) and (d) exhibit that at 18 μm, most of the absorption of the incident energy occurs between the two metal particle layers, and the bottom resonator does not contribute to the absorption.

On the other hand, when the incident wavelength is at 26 μm, the magnetic field is strongly localized between the bottom metal layer and the first metal particle layer. Obviously, the change of the top metal particle length from 5 μm to 6 μm, does not influence the absorption maximum at 26 μm or 30.5 μm activated by the bottom resonator with 7 or 8 μm as the metal particle

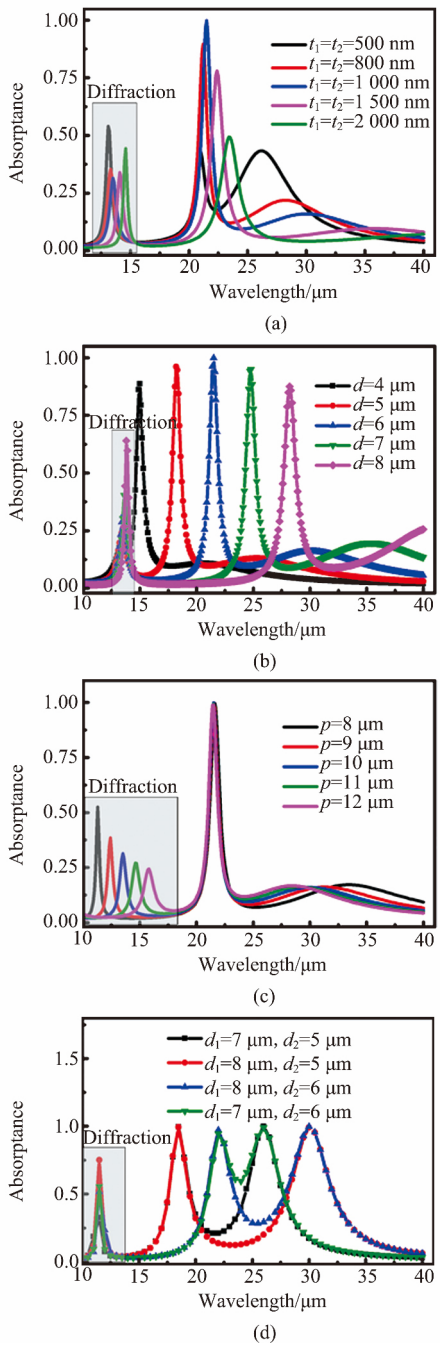

Fig. 4　The simulated absorptance as a function of wavelength and the thickness of dielectric layer (a), the side lengths of gold particle (b), the periods of gold particle (c) for this double-resonant layer absorber (d) Absorption spectrum of varying the side lengths of gold particle at the top and bottom layers

图 4　双谐振腔吸收器中，模拟的吸收率与波长和介质层厚度的关系(a)，金属块的边长(b)和金属块的周期(c)，(d)模拟改变上下两层金属块边长的吸收谱

length. This phenomenon also works the other way round, when the change of the bottom metal particle length from 7 μm to 8 μm does not influence the absorp-

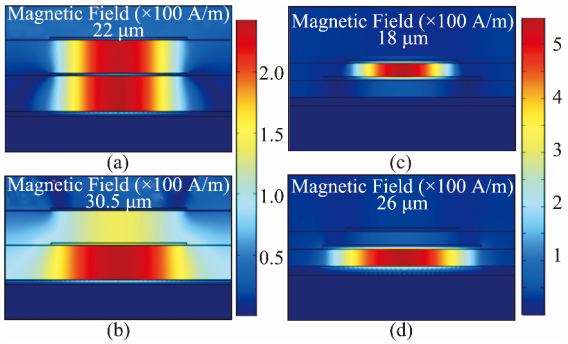

Fig. 5　(a) and (b) are the magnetic field distribution profile corresponding to the the incident wavelength of 22 μm and 30.5 μm, respectively, for the double-resonant layer absorber with $t_1 = t_2 = 1\,000$ nm, $d_1 = d_2 = 6$ μm, and $p = 10$ μm; (c) and (d) are the magnetic field distribution profile corresponding to the the incident wavelength of 18 μm and 26 μm, respectively, for the double-resonant layer absorber with $t_1 = t_2 = 1\,000$ nm, $d_1 = 7$ μm and $d_2 = 5$ μm, and $p = 10$ μm

图 5　对应于入射波长为 (a) 22 μm，(b) 30.5 μm 时的双谐振腔吸收器剖面场分布图. 对应的参数为：$t_1 = t_2 = 1\,000$ nm，$d_1 = d_2 = 6$ μm，and $p = 10$ μm. 对应于入射波长(c) 18 微米和(d) 26 μm 时的双谐振腔吸收器剖面场分布图. 对应的参数为 $t_1 = t_2 = 1\,000$ nm，$d_1 = 7$ μm and $d_2 = 5$ μm，and $p = 10$ μm

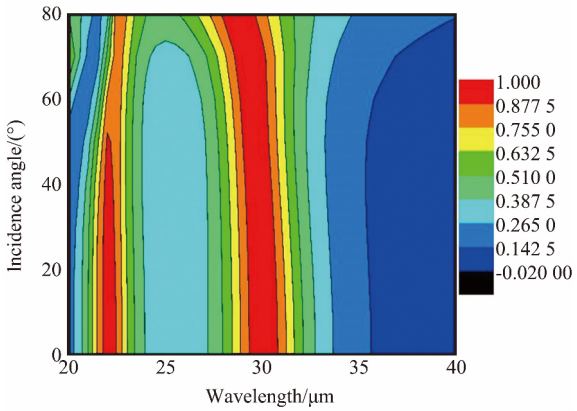

Fig. 6　Aborptance as a function of wavelength and the incident angle of light for double-resonant layer absorber with $t_1 = t_2 = 1\,000$ nm, $d_1 = 8$ μm and $d_2 = 6$ μm, and $p = 10$ μm

图 6　双谐振腔吸收器中，吸收率与入射光波长和角度的关系

tion maximum at 18 and 22 μm corresponding to the optimized top metal particle length. So, it can be concluded that with the fine-tuning of the parameters for the double-layer MA absorber, the both resonator can be independently activated for the specific wavelength, as have seen in Fig. 2(c). We believe the rather thick dielectric layer thickness might decouple the two resonators. And the LC model can work on the two resonant absorbers separately. Thus the perfect dual band absorption can be achieved, while the resonant maximum can be determined

by the LC model as discussion above.

Moreover, we further investigated the sensitivity of incident angle for the double-resonator MA absorbers with the d_1 = 8 μm, d_2 = 6 μm, and simulation results are shown in Figure 6. While both the resonant absorption maximum strength do not change significantly when the incident angle is smaller than 50°, the absorption rate at short wavelength drops much faster than the one at longer wavelength. On the other hand, the maximum at 26 μm is rather stable even with incident angle reaching 80°, although a sight blue shift occurs for the maximal position.

3 Summary

In conclusion, we have demonstrated a design of multi-layer MAs in the far-infrared regime, which can achieve an ultrahigh absorption rate, even at large incident angles. It can be attributed to the superposition of multiple magnetic resonances tuned by the metal-dielectric-metal resonant cavities. To compare with the traditional super-absorbent materials, we use the negative photoresist SU8 as the dielectric layer here, this provide a solid foundation for the preparation of three-dimensional MA.

References

[1] Woodward R M, Cole B E, Wallace V P, *et al*. Terahertz pulse imaging in reflection geometry of human skin cancer and skin tissue [J]. *Phys. Med. Biol*, 2002, **47**(21): 3853-3863.

[2] Waters J W, Froidevaux L, Harwood R S, *et al*. The Earth observing system microwave limb sounder (EOS MLS) on the Aura satellite [J]. *IEEE Trans. Geo. Rem. Sens.*, 2006, **44**(5): 1075-1092.

[3] Appleby R, Wallace H B. Standoff detection of weaponsand contraband in the 100 GHz to 1 THz region [J]. *IEEE Trans. Antenn. Propag.*, 2007, **55**(11), 2944-2956.

[4] Nagai N, Sumitomo M, Imaizumi M, *et al*. Characterization of electron-or proton-irradiated Si space solar cells by THz spectroscopy [J]. *Semicond. Sci. Technol.*, 2006, **21**(2), 201-209.

[5] Tonouchi M. Cutting-edge terahertz technology [J]. *Nat. Photonics*, 2007, **1**(2): 97-105.

[6] Pilbratt G L, Riedinger J R, Passvogel T, *et al*. Herschel Space Observatory-An ESA facility for far-infrared and submillimetre astronomy [J]. *Astron. Astrophys.*, 2010, **518:** L1.

[7] Landy N I, Sajuyigbe S, Mock J J, *et al*. Perfect metamaterial absorber [J]. *Phys. Rev. Lett.*, 2008, **100**(20): 207402.

[8] HU Tao, Landy N I, Bingham C M, *et al*. A metamaterial absorber for the terahertz regime: Design, fabrication and characterization [J]. *Opt. Express*, 2008, **16**(10): 7181-7188.

[9] HU Tao, Bingham C M, Strikwerda A C, *et al*. Highly flexible wide angle of incidence terahertz metamaterial absorber: Design, fabrication, and characterization [J]. *Phys. Rev. B*, 2008, **78**(24): 241103.

[10] Landy N, Bingham C, Tyler T, *et al*. Design, theory, and measurement of a polarization-insensitive absorber for terahertz imaging [J]. *Phys. Rev. B*, 2009, **79**(12): 125104.

[11] WEN Qi-Ye, ZHANG Huai-Wu, XIE Yun-Song, *et al*. Dual band terahertz metamaterial absorber: Design, fabrication, and characterization [J]. *Appl. Phys. Letter*, 2009, **95**(24): 241111.

[12] MA Yong, CHEN Qin, Grant J, *et al*. A terahertz polarization insensitive dual band metamaterial absorber [J]. *Opt. Letter*, 2011, **36**(6): 945-947.

[13] Grant J, MA Yong, Saha S, *et al*. Polarization insensitive, broadband terahertz metamaterial absorber [J]. *Opt. Letter*, 2011, **36**(17): 3476-3478.

[14] YE Yu-Qian, JIN Yi, HE Sai-Ling. Omnidirectional, polarization-insensitive and broadband thin absorber in the terahertz regime [J]. *J. Opt. Soc. Am. B*, 2010, **27**(3): 498-504.

[15] Hokmabadi M P, Wilbert D S, Kung P, *et al*. Design and analysis of perfect terahertz metamaterial absorber by a novel dynamic circuit model [J]. *Opt. Express*, 2013, **21**(14): 16455-16465.

[16] WEN Qi-Ye, XIE Yun-Song, ZHANG Huai-Wu, *et al*. Transmission line model and fields analysis of metamaterial absorber in the terahertz band [J]. *Opt. Express*, 2009, **17**(22): 20256-20265.

[17] Diem M, Koschny T, Soukoulis C M. Wide-angle perfect absorber/thermal emitter in the terahertz regime [J]. *Phys. Rev. B*, 2009, **79**(3): 033101.

[18] HAO Jia-Ming, ZHOU Lei, QIU Min. Nearly total absorption of light and heat generation by plasmonic metamaterials [J]. *Phys. Rev. B*, 2011, **83**(16): 165107.

[19] HAO Jia-Ming, WANG Jing, LIU Xian-Liang, *et al*. High performance optical absorber based on a plasmonic metamaterial [J]. *Appl. Phys. Letter*, 2010, **96**(25): 251104.

[20] Hendrickson J, GUO Jo-Shua, ZHANG Bo-Yang, *et al*. Wideband perfect light absorber at midwave infrared using multiplexed metal structures [J]. *Opt. Letter*, 2012, **37**(3): 371-373.

[21] Nath J, Maukonen D, Smith E, *et al*. Thin-film, wide-angle, design-tunable, selective absorberfrom near UV to far infrared [J]. *Proc. SPIE*, 2013, 8704 87041D.

[22] WANG Xiao-Nong, LUO Chun-Rong, *et al*HONG Gang, . Metamaterial optical refractive index sensor detected by the naked eye [J]. *Appl. Phys. Letter*, 2013, **102**(9): 091902.

[23] CHEN Hou-Tong. Interference theory of metamaterial perfect absorbers [J]. *Opt. Express*, 2012, **20**(7): 7165-7172.

[24] PENG Xiao-Yu, WANG Bin, LAI Shu-Min, *et al*. Ultrathin multiband planar metamaterial absorber based on standing wave resonances [J]. *Opt. Express*, 2012, **20**(25): 27756-27765.

[25] LIU Na, Mesch M, Weiss T, *et al*. Infrared Perfect Absorber and Its Application As Plasmonic Sensor [J]. *Nano Letter*, 2010, **10:** 2342.

[26] CHENG Deng-Mu, XIE Jian-Liang, ZHANG Hui-Bing, *et al*. Pantoscopic and polarization-insensitive perfect absorbers in the middle infrared spectrum [J]. *J. Opt. Soc. Am. B*, 2012, **29:** 1503.

[27] Ordal M A, Long L L, Bell R J, . Optical properties of the metals Al, Co, Cu, Au, Fe, Pb, Ni, Pd, Pt, Ag, Ti, and W in the infrared and far infrared [J]. *Appl. Opt.*, 1983, **22:** 1099.